Realization of a Strongly Nonlinear Vibration-Mitigation Device Using Elastomeric Bumpers

Jie Luo, S.M.ASCE[1]; Nicholas E. Wierschem, S.M.ASCE[2]; Larry A. Fahnestock, P.E., M.ASCE[3]; Lawrence A. Bergman, M.ASCE[4]; Billie F. Spencer Jr., P.E., F.ASCE[5]; Mohammad AL-Shudeifat[6]; D. Michael McFarland[7]; D. Dane Quinn[8]; and Alexander F. Vakakis[9]

Abstract: Recent research has shown the viability of using nonlinear energy-sink (NES) devices for vibration mitigation in mechanical and structural systems. When attached to a primary structure, these lightweight passive devices can effectively reduce the structural vibration response through their nonlinear stiffness properties. In this research, a two-degree-of-freedom NES device is designed using innovative elastomeric bumpers as the critical components providing nonlinear restoring forces. A number of elastomeric bumper configurations are evaluated experimentally, and the effect of geometric bumper parameters is investigated with a focus on their influence on the stiffness properties of the bumper. A NES device employing different bumpers is then implemented on a 6-story model building and tested using impulse-like base motion. Nonlinear system identification of the NES device shows that nonlinear stiffness properties are achieved using the elastomeric bumpers. Shake-table testing of the building equipped with the NES device demonstrates that the device is capable of dissipating and redistributing the induced vibration energy in a rapid, effective, and robust fashion. **DOI: 10.1061/(ASCE)EM.1943-7889.0000692.**

Author keywords: Passive control; Nonlinear systems; Damping; Impulsive loads; Dynamic tests; Foam; Nonlinear energy sink; Elastomeric bumper; Targeted energy transfer.

Introduction

Analytical, numerical, and experimental studies conducted over the last decade have demonstrated the efficacy of nonlinear energy-sink (NES) devices for vibration mitigation in mechanical and structural systems (McFarland et al. 2005a; Gourdon et al. 2007; Kerschen et al. 2007; Quinn et al. 2008, 2012; Sapsis et al. 2009; Wierschem et al. 2012b). These passive devices are lightweight vibration absorbers that exhibit essentially nonlinear stiffness (i.e., there is no linear term in the force-displacement relationship) and thus have no preferential resonant frequency. As a result, a NES device can interact with multiple structural modes to passively absorb and locally dissipate vibration energy of the structure to which it is attached. This one-way and nearly irreversible energy flow from the primary structure to the local NES device has been studied as targeted energy transfer (TET) (Gendelman et al. 2000; Vakakis and Gendelman 2000; Vakakis et al. 2004; McFarland et al. 2005b; Vakakis et al. 2008). Besides absorbing and dissipating vibration energy by itself, the NES device can also redistribute the vibration energy from low-frequency structural modes to high-frequency modes by coupling the linear structural modes together (Quinn et al. 2012). Thus vibration response of the primary structure, e.g., resulting from shock or earthquake loading, can be effectively mitigated through the action of the NES device.

A number of NES devices have been investigated, and two of the primary configurations are illustrated schematically in Fig. 1. As shown in Fig. 1(a), the simplest configuration is the Type I NES, and it consists of a single-degree-of-freedom attachment with nonlinear stiffness and linear viscous damping (McFarland et al. 2005a; Quinn et al. 2012). The nonlinear stiffness has typically been introduced using transverse linear springs, such as a linear elastic wire with no slack or pretension. Thus the transverse restoring force f_{res} is a function of the transverse relative displacement between the NES mass and the primary structure x_{rel}, where the exact force-displacement relationship can be derived as

$$f_{res}(x_{rel}) = \frac{EA}{L^3}x_{rel}^3 + O(x_{rel}^5) \quad (1)$$

where E and A = wire modulus of elasticity and cross-sectional area, respectively; and L = length of the wire on one side of the mass. The

[1]Graduate Research Assistant, Dept. of Civil and Environmental Engineering, Univ. of Illinois at Urbana-Champaign, Urbana, IL 61801. E-mail: jieluo2@illinois.edu

[2]Graduate Research Assistant, Dept. of Civil and Environmental Engineering, Univ. of Illinois at Urbana-Champaign, Urbana, IL 61801 (corresponding author). E-mail: nwiersc2@illinois.edu

[3]Associate Professor, Dept. of Civil and Environmental Engineering, Univ. of Illinois at Urbana-Champaign, Urbana, IL 61801. E-mail: fhnstck@illinois.edu

[4]Professor, Dept. of Aerospace Engineering, Univ. of Illinois at Urbana-Champaign, Urbana, IL 61801. E-mail: lbergman@illinois.edu

[5]Nathan M. and Anne M. Newmark Endowed Chair in Civil Engineering, Dept. of Civil and Environmental Engineering, Univ. of Illinois at Urbana-Champaign, Urbana, IL 61801. E-mail: bfs@illinois.edu

[6]Assistant Professor, Dept. of Aerospace Engineering, Khalifa Univ. of Science, Technology and Research, P.O. Box 127788, Abu Dhabi, UAE. E-mail: mohd.shudeifat@kustar.ac.ae; formerly, Postdoctoral Research Associate, Dept. of Mechanical Science and Engineering, Univ. of Illinois at Urbana-Champaign, Urbana, IL 61801. E-mail: shdefat@illinois.edu

[7]Research Associate Professor, Dept. of Aerospace Engineering, Univ. of Illinois at Urbana-Champaign, Urbana, IL 61801. E-mail: dmmcf@illinois.edu

[8]Professor, Dept. of Mechanical Engineering, Univ. of Akron, Akron, OH 44325. E-mail: quinn@akron.edu

[9]W. Grafton and Lillian B. Wilkins Professor, Dept. of Mechanical Science and Engineering, Univ. of Illinois at Urbana-Champaign, Urbana, IL 61801. E-mail: avakakis@illinois.edu

Note. This manuscript was submitted on March 27, 2012; approved on July 8, 2013; published online on July 10, 2013. Discussion period open until June 7, 2014; separate discussions must be submitted for individual papers. This paper is part of the ***Journal of Engineering Mechanics***, © ASCE, ISSN 0733-9399/04014009(11)/$25.00.

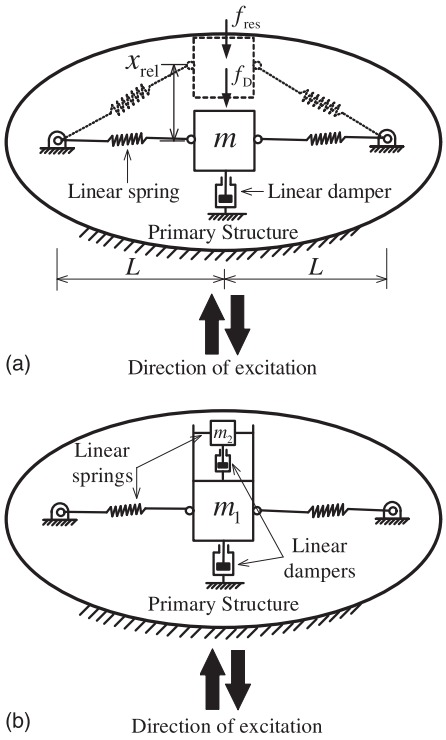

Fig. 1. Schematic configurations of Type I and Type III NES devices using transverse linear springs: (a) Type I NES device; (b) Type III NES device

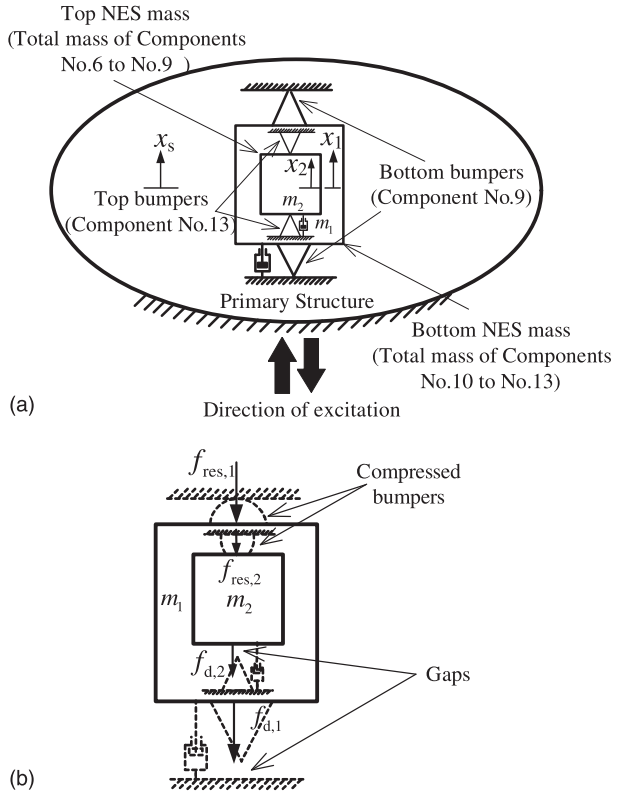

Fig. 2. Schematic operating condition and force diagram of Type III NES device using elastomeric bumpers: (a) schematic configuration [key components are labeled in conjunction with Fig. 3(a) and Table 1]; (b) force diagram in operating condition

key feature of this force-displacement relationship is the essential nonlinearity, in this case dominated by the cubic term.

As shown in Fig. 1(b), the Type III NES device is a two-degree-of-freedom device that is composed of nested Type I NES devices (Quinn et al. 2012; Wierschem et al. 2012b). Although the transverse wire configuration described earlier for realizing smooth essential nonlinearity in NES devices has proven to be effective in bench-scale laboratory tests, it is not necessarily a realistic approach for NES devices implemented in large-scale structures. Thus, alternative approaches for achieving essential nonlinear stiffness are critical for transferring the NES technology into civil infrastructure systems.

This research explores the use of elastomeric bumpers as the essential nonlinear restoring-force components of the NES device. Elastomeric materials, including various rubbers, plastics, and foams, have been studied and employed in the field of vibration isolation and mitigation because of their unique engineering properties (e.g., Corsaro and Sperling 1990; Gibson and Ashby 1997; Gent 2001). In this study, an innovative Type III NES device using pairs of elastomeric polyurethane foam bumpers is developed and experimentally validated. Fundamental material characterization of the elastomeric polyurethane foam was conducted, and compression tests of foam bumpers were used to study the variations in nonlinear stiffness behavior as a function of geometric bumper parameters. Nonlinear system identification of the Type III NES device with elastomeric bumpers demonstrates that the desired essentially nonlinear stiffness properties can be achieved through the combination of material and geometric nonlinearity. Shake-table testing of a model 6-story building using impulse-like loading illustrates the capability of NES devices with elastomeric bumpers for providing vibration mitigation by rapidly dissipating and redistributing high levels of input energy. This research is part of an extensive program that is investigating NES devices for vibration mitigation, and aspects of this research related to device design are for the purpose of achieving optimized building system performance (Wierschem et al. 2012a).

Type III Nonlinear Energy Sink with Elastomeric Bumpers

As discussed earlier and illustrated in Fig. 1(b), in previous work the Type III NES device has been physically realized using transverse linear springs to create a cubic load-displacement term. Fig. 2(a) schematically illustrates the new NES device configuration considered in this research. Two pairs of tailored elastomeric bumpers create the nonlinear restoring forces in the two-degree-of-freedom device. The bumpers are placed in the direction of motion of the NES masses, and at rest, the bumpers are exactly in contact with the NES masses but are not precompressed. Fig. 2(b) illustrates the deformation of the bumpers when the NES masses undergo relative displacements, along with the corresponding force diagram of this operating condition. Under excitation, the bumper on one side of the mass will be compressed, whereas a gap opens on the other side of the mass. The deformed bumper will apply a nonlinear restoring force f_{res} on the NES mass that is compressing it. A linear viscous damping force f_d is assumed for each mass to model the various damping sources, which include the frictional damping on the shafts and rails and the material damping of the bumpers. As an alternative source of the nonlinear restoring force, the use of bumpers creates a NES design that is compact, reliable, and most important, practical to be implemented in large-scale civil structures.

Consider the system of a Type III NES device attached to a primary structure. As shown in Fig. 2(a), the physical coordinates

describing the bottom and top NES masses are denoted by x_1 and x_2, respectively. The coordinate of the primary structure at the location of NES device attachment is described by x_s. In the operating condition, the equations of motion (EOMs) governing the device can be written as

$$m_1\ddot{x}_1 = -f_{\text{NES},1}(x_s,\dot{x}_s,x_1,\dot{x}_1) + f_{\text{NES},2}(x_1,\dot{x}_1,x_2,\dot{x}_2) \quad (2a)$$

$$m_2\ddot{x}_2 = -f_{\text{NES},2}(x_1,\dot{x}_1,x_2,\dot{x}_2) \quad (2b)$$

where $f_{\text{NES},1}(x_s,\dot{x}_s,x_1,\dot{x}_1)$ and $f_{\text{NES},2}(x_1,\dot{x}_1,x_2,\dot{x}_2)$ = coupling force between the first NES mass m_1 and the primary structure and coupling force between the two NES masses m_1 and m_2, respectively. As shown in Fig. 2(b), these coupling forces are the combination of a linear viscous damping force f_d and a nonlinear restoring force f_{res}, which can be described by an exponential function. Consequently, these coupling forces can be calculated by

$$\begin{aligned} f_{\text{NES},1}(x_s,\dot{x}_s,x_1,\dot{x}_1) &= f_{d,1} + f_{\text{res},1} \\ &= c_{\text{NES},1}(\dot{x}_1 - \dot{x}_s) \\ &\quad + k_{\text{NES},1}\text{sgn}(x_1 - x_s)|x_1 - x_s|^{\alpha_1} \end{aligned} \quad (3a)$$

$$\begin{aligned} f_{\text{NES},2}(x_1,\dot{x}_1,x_2,\dot{x}_2) &= f_{d,2} + f_{\text{res},2} \\ &= c_{\text{NES},2}(\dot{x}_2 - \dot{x}_1) \\ &\quad + k_{\text{NES},2}\text{sgn}(x_2 - x_1)|x_2 - x_1|^{\alpha_2} \end{aligned} \quad (3b)$$

where $c_{\text{NES},i}$ and $k_{\text{NES},i}$ = damping and stiffness coefficients associated with the ith stage of the NES device, respectively; and α_i = exponent of the nonlinear stiffness term of the ith stage of the NES device.

Fig. 3 shows the laboratory realization of the Type III NES device depicted schematically in Fig. 2. The item numbers in Figs. 2 and 3(a) correspond to the detailed descriptions in Table 1. As shown in Fig. 3(b), this NES device is composed of two stages, where motion occurs uniaxially in the direction of excitation. The top stage of moving mass in Fig. 2 is realized using a 200-mm-tall rectangular steel tube with additional masses secured inside, which is nested inside the bottom stage, and has a total mass of 21 kg. The steel tube is installed on top of bearings that travel on a rail fixed to the baseplate of the bottom stage. The steel tube alternately compresses the bumpers on either side as the direction of motion changes. The realization of the bottom NES mass shown in Fig. 2, which has a total mass of 28 kg, consists primarily of a $500 \times 330 \times 12.5$-mm baseplate and two $360 \times 330 \times 12.5$-mm vertical aluminum plates. Four bushing bearings installed beneath the baseplate facilitate the motion of this stage along two parallel shafts fixed on top of the primary structure. The bottom elastomeric bumpers are compressed between the vertical plates and angles that are attached to the top-floor plate of the primary structure. As noted earlier, at the static equilibrium position of each stage, the bumpers just contact the plates that will compress them, and there is no gap or precompression.

Material Characterization

Compression testing of high-resilience polyurethane open-cell foam specimens was performed at the Advanced Materials Testing and Evaluation Laboratory at the University of Illinois at Urbana-Champaign using a 13-kN servocontrolled hydraulic test frame. To investigate the fundamental mechanical properties of the material, five polyurethane foam specimens of different firmness were tested under monotonic uniaxial compression at a relatively slow (quasi-static) loading rate of 1 mm/s. All the specimens are $175 \times 175 \times 100$-mm prismatic rectangular blocks, and they were compressed in the 100-mm direction. Fig. 4 shows the nominal stress-strain curves that were obtained for all specimens. These results are consistent with prior research on the compressive response of foams (e.g., Wierzbicki and Doyoyo 2003; Gong et al. 2005; Gong and Kyriakides 2005). The change in behavior for different levels of foam firmness is evident, and all specimens exhibit several characteristic stages of response.

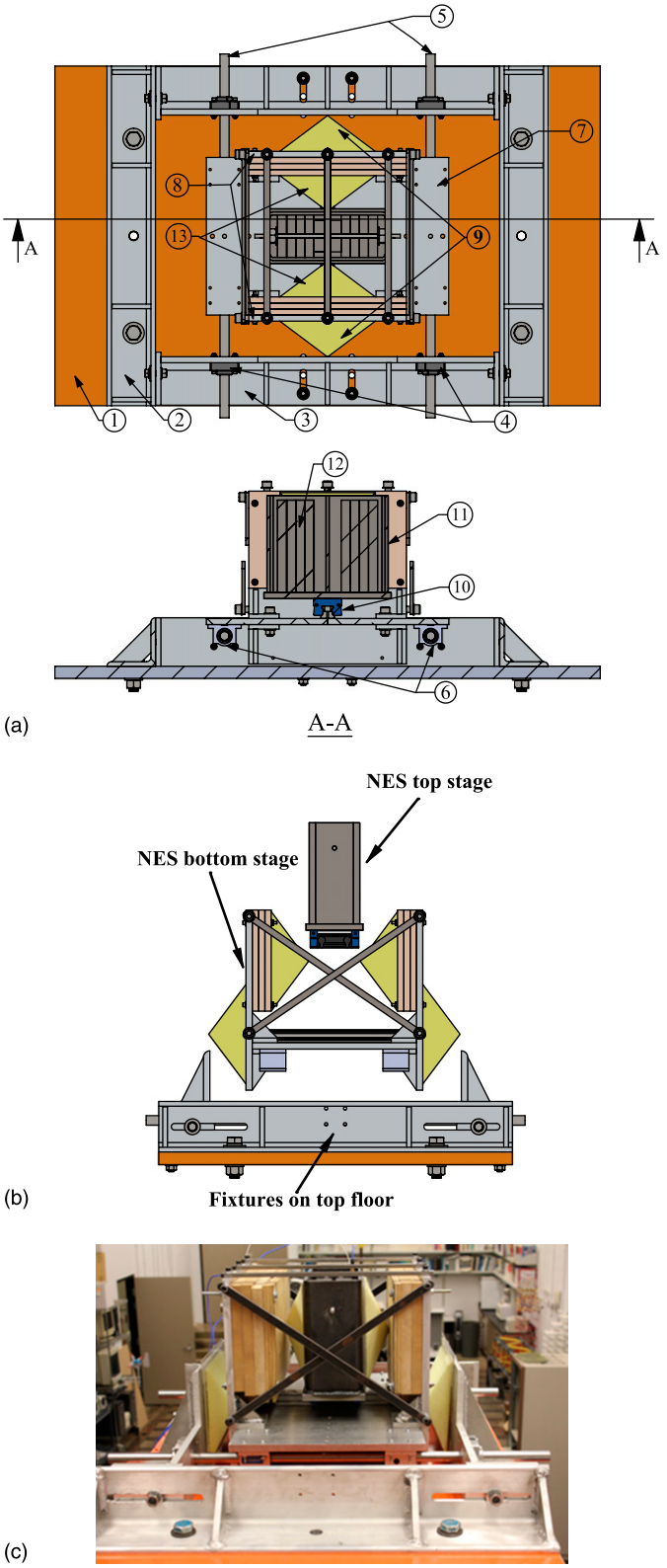

Fig. 3. Type III NES device laboratory realization: (a) plan and section; (b) exploded elevation; (c) photograph

Table 1. Components of Type III NES Device Laboratory Realization

Part	Number	Component
NES device housing	1	Primary structure floor plate
	2	Aluminum angle (longitudinal)
	3	Aluminum angle (transverse)
	4	Shaft support block
	5	Round stainless-steel shaft
NES device bottom stage	6	Bearing pillow block
	7	Aluminum-alloy base plate
	8	Vertical aluminum plates
	9	Bottom elastomeric bumpers
NES device top stage	10	Carriage and rail
	11	Steel tube section
	12	Additional steel blocks
	13	Top elastomeric bumper

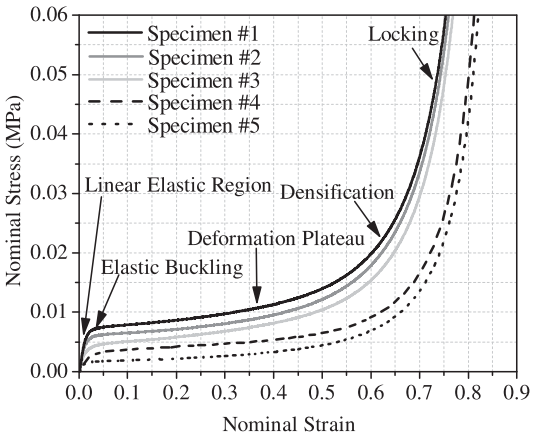

Fig. 4. Nominal monotonic stress-strain behavior of polyurethane foam (from Specimen 5 to Specimen 1, the material becomes firmer)

1. In the initial stage with small stress and strain (<0.05), the material deforms linearly as a result of the elastic bending of micro cell walls.
2. Shortly after the proportional limit, a deformation plateau with low stiffness is observed as a result of elastic buckling of micro cell walls.
3. As the strain increases beyond roughly 0.6, a densification stage occurs as a result of the crushing of cell walls, and the stiffness increases rapidly.
4. At a nominal compressive strain of 0.8–0.9, a locking phenomenon is observed with sharply increasing stiffness.

To investigate the dynamic behavior of the polyurethane foam, Specimen 3 was tested under cyclic uniaxial compression using a sinusoidal displacement protocol with a frequency of 1 Hz. This loading frequency was chosen to approximate the expected operating frequency of the NES device based on numerical simulation results. Seven complete cycles were performed during the test. Fig. 5 illustrates the cyclic stress-strain response of the polyurethane foam. After the first cycle, the curves corresponding to different cycles are essentially overlapping in both loading and unloading phases, which shows that the material is able to recover its undeformed shape rapidly and thus exhibits stable and repeatable cyclic behavior. The loading phase of the cyclic curves also shows good agreement with the quasi-static loading curve for the same specimen, as shown in Fig. 5, which indicates that the stiffness of the material is not sensitive to this loading rate.

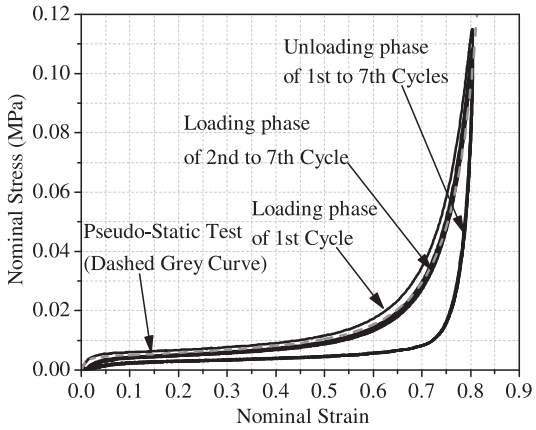

Fig. 5. Nominal cyclic stress-strain behavior of polyurethane foam

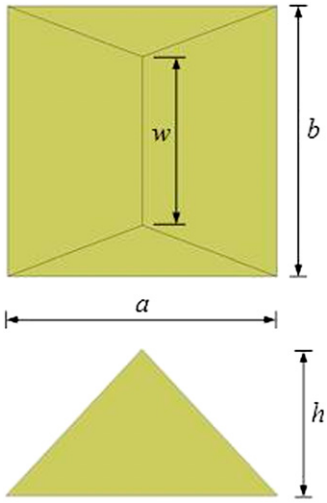

Fig. 6. Bumper geometric parameters

Therefore, characterization of load-displacement behavior for the bumper specimens discussed in subsequent sections is conducted using quasi-static loading.

Parametric Study of Bumper Geometry

To evaluate options for achieving the strongly nonlinear load-displacement behavior that is required for the nonlinear spring elements in a NES device, polyurethane foam bumpers with different geometries were tested. Bumpers with base dimensions a and b were considered, and focus was placed on two geometric parameters that have significant influence on behavior: height h and top width w. Fig. 6 illustrates these geometric parameters for a bumper. In this research, when the top width w is equal to the bottom width b, the bumper is called wedge shaped. At the other extreme, when the top width w is equal to zero, the bumper is called pyramid shaped. A bumper with w between zero and b is called hybrid shaped. Table 2 summarizes the geometric properties of the bumpers that were tested.

Fig. 7 shows the experimental setup designed to simulate the demands on the bumpers as the compressive stiffness components in the NES device. Before testing, the bumper specimen is firmly glued on top of a bottom platen, and the bumper tip is just in contact with

Table 2. Bumper Test Matrix

Label	a (mm)	b (mm)	w (mm)	h (mm)
W1	200	200	200	50
W2	200	200	200	62.5
W3	200	200	200	75
W4	200	200	200	87.5
W5	200	200	200	100
P1	200	200	0	37.5
P2	200	200	0	50
P3	200	200	0	62.5
P4	200	200	0	75
P5	200	200	0	87.5
H1	200	200	150	75
H2	200	200	100	75
H3	200	200	50	75

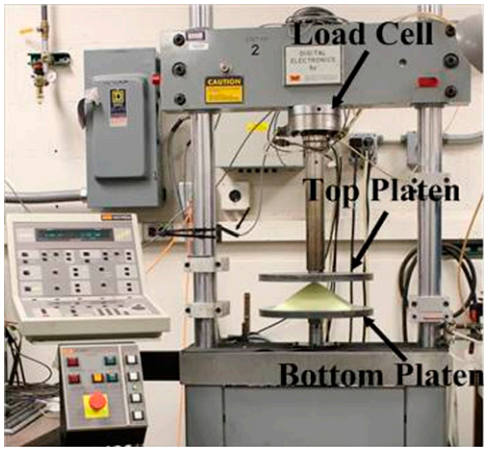

Fig. 7. Experimental setup of uniaxial compression tests on bumper specimens

a top platen that is connected to a load cell. When the actuator pushes the bottom platen upward, the top platen is held fixed and uniformly compresses the bumper from its top in the height direction. The displacement of the bottom platen and the compressive force transferred to the load cell are measured and reported as the compressive displacement and compressive load in Figs. 8–10. The compressive load in these tests corresponds with the nonlinear restoring force f_{res} shown in Fig. 2(b) and Eq. (3). For all these test results, a quasi-static monotonic loading with a rate of 1 mm/s was used to control the compressive loading. Under this slow loading rate, the nonlinear restoring force f_{res} can be tested without consideration of the damping force f_d.

Effect of Bumper Height

Experimental results show that the height of the bumper plays a key role in altering its load-displacement behavior. Five wedge-shaped polyurethane foam bumpers (labeled W1–W5) made of the same material as Specimen 1 described earlier (the foam with the highest firmness) were tested. All these bumpers had a square base and a full top width ($a = b = w = 200$ mm) but different heights (h from 50 to 100 mm).

Comparison was made between the stress-strain behavior shown in Fig. 4, which has the same shape as load-displacement behavior for a prismatic rectangular block of foam, and the load-displacement behavior of the wedge-shaped bumpers in Fig. 8. The comparison

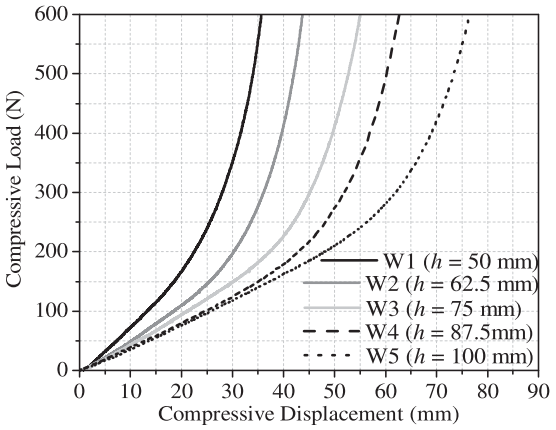

Fig. 8. Load-displacement behavior of wedge-shaped ($w = b$) bumpers with variation in height h

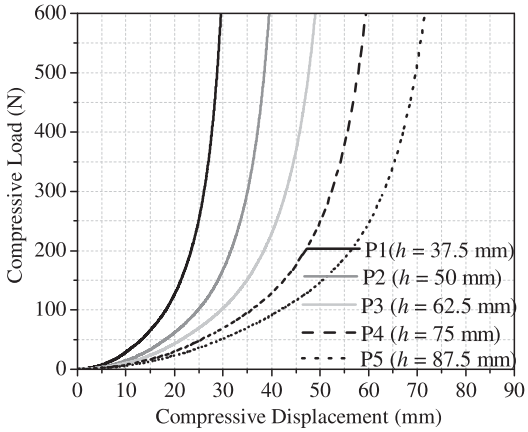

Fig. 9. Load-displacement behavior of pyramid-shaped ($w = 0$) bumpers with variation in height h

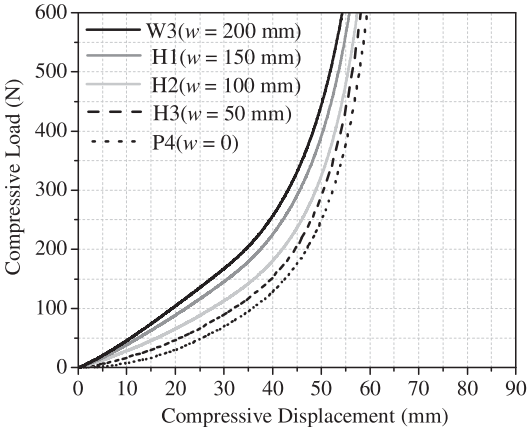

Fig. 10. Load-displacement behavior of bumpers with variation in top width w

shows that the tapered bumper geometry eliminates the sudden transition in stiffness resulting from the elastic buckling and leads to behavior with monotonically increasing stiffness. As bumper height increases, bumper stiffness decreases. This relationship is beneficial for tuning bumper properties to achieve desired stiffness

parameters for NES device design. Although the global nonlinear load-displacement behavior with monotonically increasing stiffness is desirable for NES device design, a region of nearly constant stiffness shown by the linear load-displacement relationship exists locally in the early portions of the load-displacement curve. This constant stiffness is undesirable for NES device design because the fundamental behavior of the device is based on essentially nonlinear stiffness. To reduce this constant-stiffness component and increase the nonlinearity of the bumpers, further tuning of the bumper geometry is required.

Effect of Bumper Top Width

Additional nonlinearity in bumper behavior can be achieved by reducing the contact area at the top of the bumper. Whereas wedge-shaped bumpers have line contact, the point contact of pyramid-shaped bumpers can realize a minimum possible initial contact. Thus five pyramid-shaped bumpers (labeled P1–P5) that were made of the same polyurethane foam as the wedge-shaped bumpers were tested. These bumpers had a square base ($a = b = 200$ mm), a pointed top ($w = 0$), and different heights (h from 37.5 to 87.5 mm). The load-displacement curves for these specimens are shown in Fig. 9. As expected, the stiffness still increases monotonically, and the region of constant stiffness that was observed for the wedge-shaped bumpers is eliminated. Similar to the wedge-shaped bumpers, the bumper height of the pyramid-shaped bumpers plays a key role in determining the global stiffness, but the overall behavior is highly nonlinear, even for bumpers with low height.

To examine the variation in behavior between wedge- and pyramid-shaped bumpers, three additional hybrid-shaped bumpers (labeled H1–H3) were tested. These bumpers had a square base ($a = b = 200$ mm), a constant height ($h = 75$ mm), but different top widths (w from 50 to 150 mm). Thus these bumpers fill the parametric space between Bumpers W3 and P4. Fig. 10 shows the load-displacement curves for W3 and P4 along with H1–H3. The effect of top width on the overall stiffness is less significant than that of bumper height, but as shown by the comparison between wedge- and pyramid-shaped bumpers, the top width significantly influences the degree of nonlinearity in the load-displacement behavior. As the top width decreases, the response becomes more nonlinear, particularly in the initial region, and the desired essential nonlinearity is obtained.

Dynamic Testing of 6-Story Building with Type III NES Device

To demonstrate the efficacy of NES technology for mitigation of cyclic vibration response in civil structures, the authors developed an experimental test bed using a 6-story model building in conjunction with a shake table. A Type III NES device was installed on top of the building and tested with different configurations of elastomeric bumpers. Although the mass of the NES device is only 5% of the building mass, it is expected to increase the apparent structural damping and quickly reduce the structural vibration responses introduced by an impulse-like base excitation.

The bumper parametric study described earlier was used as a foundation for experimentally evaluating selected bumper configurations for the Type III NES device. In general, the trends identified from the bumper parametric study can be used for tuning the bumper behavior to a desired target identified through optimization of the primary structure response. The results presented in the following sections are not targeted to achieve a particular optimized case but rather to illustrate the variation in primary-system behavior as the NES device properties are modified. The effectiveness of the Type III NES device for reducing the vibration of a linear primary structure under impulse-like loading is highlighted. The different performance of the NES device employing wedge-, pyramid-, and hybrid-shaped bumpers, with properties as shown in Table 3, is presented.

Table 3. Bumper Properties for NES Device Designs

Type	Stage	a (mm)	b (mm)	w (mm)	h (mm)	c (N-s/m)	k (N/m^{α})	α
Wedge	Top	200	200	200	37.5	140.7	8.32×10^4	1.50
	Bottom	200	200	200	50	122.4	5.58×10^5	2.07
Pyramid	Top	175	175	0	37.5	101.1	8.11×10^8	4.09
	Bottom	200	200	0	50	116.4	6.44×10^6	2.97
Hybrid	Top	200	200	100	50	102.4	6.12×10^6	2.91
	Bottom	200	200	100	50	154.1	1.29×10^7	3.02

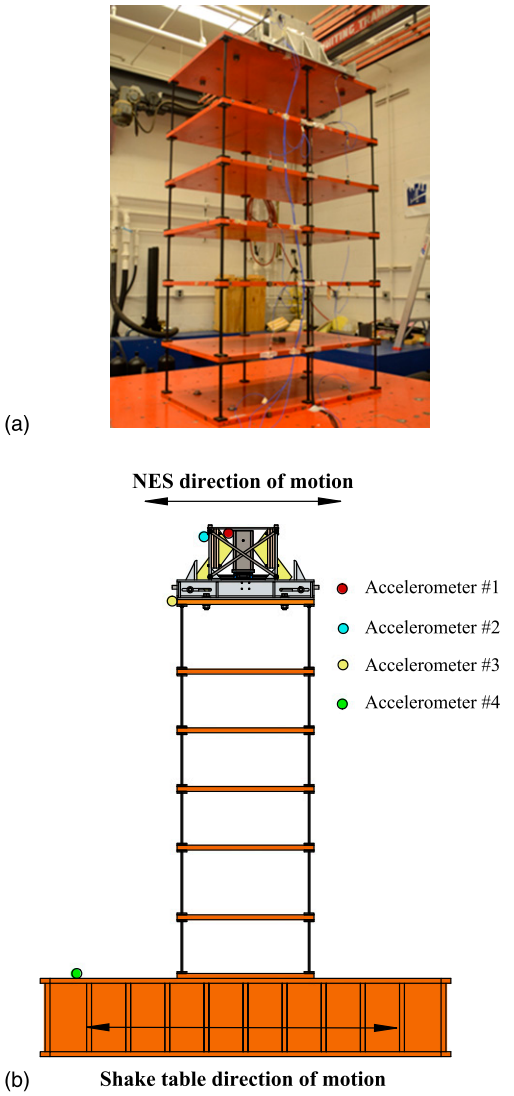

Fig. 11. Experimental setup of 6-story building with Type III NES device for shake-table testing: (a) photograph; (b) schematic diagram

Experimental Setup

Figs. 11(a and b) show the experimental setup of the shake-table testing. During a test, the shake table inputs energy to the system by

providing an impulse-like base acceleration. On top of the building, where the structural response has the largest amplitude, a Type III NES device with elastomeric bumpers is installed using the housing fixture shown in Fig. 3. The NES device is expected to absorb vibration energy from the primary structure and then dissipate the absorbed energy through its internal damping sources, including frictional damping on the shaft and rail and material damping of the elastomeric bumpers. Additionally, because of the essentially nonlinear restoring forces, the NES device is expected to couple the structural modes of the building together. As a result, the input energy to the structure is redistributed from low-frequency structural modes to high-frequency modes, which contribute little to the structural responses. Moreover, by transferring energy to the higher modes through nonlinear response, energy can be more rapidly dissipated because higher structural modes possess higher structural damping capacity. In effect, the action of the NES device is to increase the effective overall damping of the structure. This benefits structural behavior in multiple ways, including reduction of structural damage from fatigue.

The model building is composed of $711 \times 1{,}143 \times 25$-mm steel floor plates supported by high-strength steel columns. The structure is 1.97 m tall and has a total mass of 970 kg. In the direction of excitation shown in Fig. 11(b), which is along the short edge of the structural plan, the natural frequencies of the six translational modes are 1.62, 4.51, 7.46, 9.78, 11.65, and 14.43 Hz. The building is fixed on a 2.13×2.13-m shake table located in the Smart Structures Technology Laboratory at the University of Illinois at Urbana-Champaign.

Using this shake table, the structure was excited uniaxially with an impulse-like base motion. Fig. 12 shows the time-series and single-sided Fourier spectrum of this base motion. The base acceleration record is collected by Accelerometer 4 shown in Fig. 11(b). The Fourier spectrum of the input illustrates that the harmonic components of the excitation spread over a broad range of frequencies, covering all the natural frequencies of the translational structural modes. Moreover, the predominant component of the excitation is particularly designed to concentrate around the first three structural modes. This is for the purpose of sufficiently exciting the low-frequency structural modes that will lead to a relatively large displacement amplitude. Using this excitation, the performance of the NES device in regard to dissipating a broad band of input energy can be effectively evaluated.

The acceleration responses of the primary structure and the NES device were measured with PCB Model 3701G3FA3 capacitive accelerometers (PCB Piezotronics, Depew, New York). Fig. 11(b) shows the layout of the key accelerometers. The acceleration signals were collected with a VibPilot data-acquisition system (M+P International, Verona, New Jersey) using a sampling frequency of 1,024 Hz. Acceleration signals presented in the following sections were low-pass filtered to 50 Hz using an eighth-order Butterworth filter and high-pass filtered to 0.6 Hz using a fifth-order Butterworth filter. These filters perform digital filtering in both the forward and reverse directions and thus produce no phase distortion in the signal (Boore and Bommer 2005).

Nonlinear System Identification of Type III NES Device

To determine the dynamic properties of the Type III NES device using different elastomeric bumpers, a series of nonlinear system identifications were conducted with data collected during the tests. The technique used for this experimental identification is the restoring-force surface method (Masri and Caughey 1979), which is based on the equations of motion shown in Eqs. (2) and (3).

For example, the coupling force associated with the NES device top stage is a function of $\dot{x}_2$, x_2, $\dot{x}_1$, and x_1 (the velocity and displacement of the NES device top and bottom stages), which can be estimated from experimentally collected accelerations by Accelerometers 1 and 2 shown in Fig. 11(b). Because the NES device top-stage mass is known and the acceleration can be measured, the generalized coupling force on the left-hand side of Eq. (2*b*) can be calculated at all times. This known generalized coupling force can then be set equal to the assumed form on the right-hand side of Eq. (2*b*), where the parameters to be identified are damping coefficient $c_{\mathrm{NES},1}$, stiffness component $k_{\mathrm{NES},1}$, and order of the nonlinear stiffness α_1. With the calculated general coupling force and estimated displacements and velocities, the parameters in this model can be determined from a best fit to complete the identification of the system associated with the NES device top stage. A similar procedure is used to identify the parameters of the NES device bottom stage.

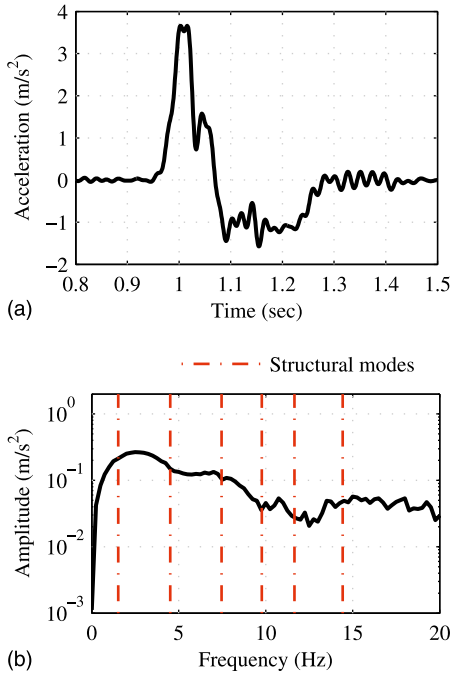

Fig. 12. Impulse-like base acceleration input: (a) time series; (b) single-sided Fourier spectrum

Table 3 summarizes the results of the system identifications for the three bumper configurations. In Fig. 13, the identified model of the nonlinear restoring force from the nonlinear stiffness components of the top and bottom NES device stages are compared for each set of bumpers. The figure shows that the three sets of bumpers have a large amount of variability in both the degree of nonlinearity that they achieve and the maximum restoring force they produce. As expected, the wedge-shaped bumpers exhibited the lowest degree of nonlinearity with α in the 1.5–2.0 range. Hybrid-shaped bumpers can be used to achieve the desired ideal cubic load-displacement relationship ($\alpha = 3.0$) in NES device designs with transverse linear springs, and pyramid-shaped bumpers can achieve an even higher degree of nonlinearity ($\alpha > 4.0$).

Response of Structure-Device System to Impulse-Like Base Motion

The 6-story model building was subjected to the impulse-like base acceleration shown in Fig. 12 to demonstrate the variation in system performance with different NES device configurations. Type III NES device designs with the three different bumper sets shown in Table 3 were considered, and the building was also tested for the

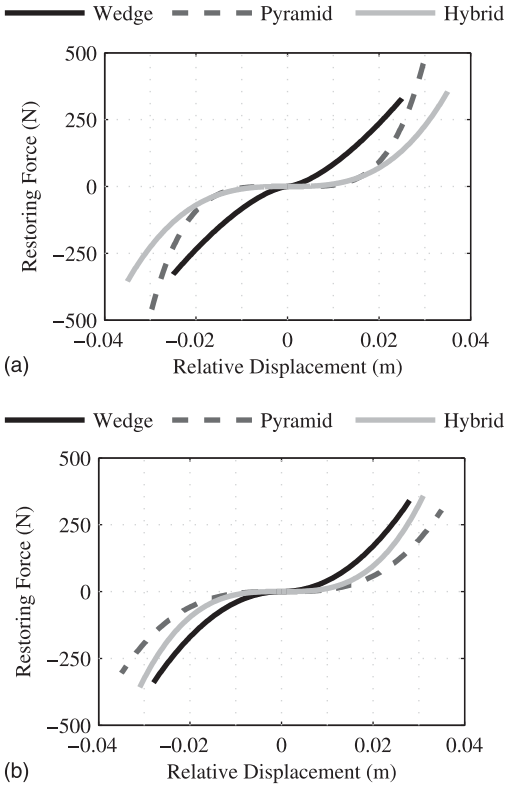

Fig. 13. Restoring-force behavior of NES device with different bumper configurations: (a) top stage; (b) bottom stage

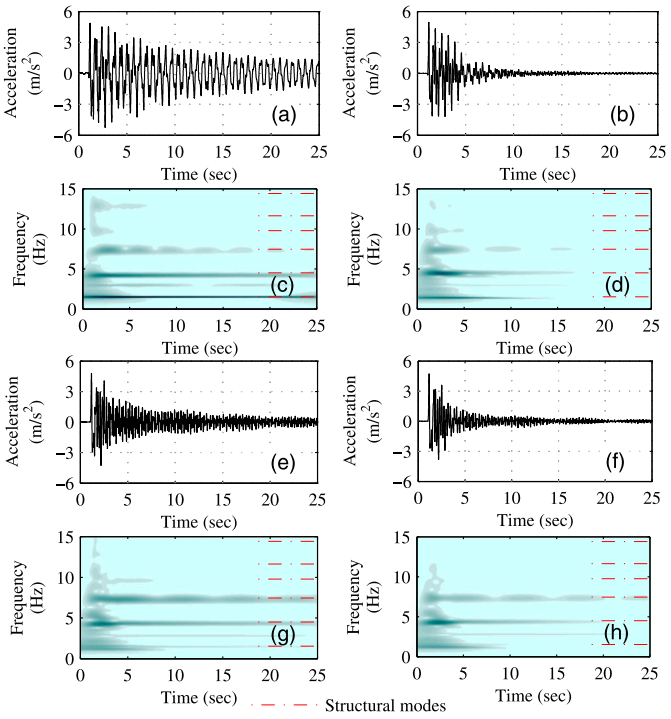

Fig. 14. Time series and wavelet spectra of building-top acceleration from experiments with NES devices with different bumper configurations: (a) and (c) NES device locked; (b) and (d) NES device with wedge-shaped bumpers; (e) and (g) NES device with pyramid-shaped bumpers; (f) and (h) NES device with hybrid-shaped bumpers

baseline case with the NES device locked (i.e., both NES device masses were prevented from moving such that the NES device was inactivated).

Fig. 14 shows the acceleration response of the top floor of the building for these four cases, collected from Accelerometer 3 shown in Fig. 11(b). Although the maximum acceleration response is largely unchanged in all cases, the three cases with activated NES devices exhibit appreciably greater apparent damping, and the amplitudes of the responses are reduced to a low level within the first several seconds. However, for the case with the locked NES device, the amplitude of the response was still significant after 25 s of vibration. In addition to the time-domain response, wavelet spectra shown in Figs. 14(c, d, g, and h) are used to provide insight into the structural response in the time-frequency domain. Note that in these figures the plots of the four wavelet spectra are correlated in the sense that the darkest and lightest shadows in the plots represent the highest and lowest amplitudes of the spectra across all four cases. Among the four spectra, the frequency component of the fundamental mode in the locked case is most predominant, and it lasts for the longest time, shown by the darkest and longest shadow along the horizontal line marking the fundamental frequency. By contrast, in every unlocked case, both the amplitude and duration of the first-mode component are substantially reduced because of the motion of the NES device. Similarly, alleviation of the second-mode component can also be observed in the unlocked cases, although it is less effective than that of the first-mode response. Additionally, the redistribution of vibration energy can be clearly observed in the unlocked case with pyramid-shaped bumpers, which has the highest nonlinearity. The third-mode response shown in Fig. 14(g) is strengthened compared with that of the locked case in Fig. 14(c). This indicates that besides absorbing and dissipating vibration energy, this essentially nonlinear device is also capable of redistributing energy from low-frequency to high-frequency modes that contribute little to the displacement response of the structure.

Although the NES device configurations employing different elastomeric bumpers all exhibit robust performance for mitigating vibration response, differences in the performances of the three sets of bumpers need to be further examined. The NES devices with pyramid- and hybrid-shaped bumpers have similar performances in mitigating the first-mode vibration, judging by the similar responses of the fundamental mode shown in Figs. 14(g and h). However, the NES device equipped with pyramid-shaped bumpers redistributes more vibration energy to the third mode than does the NES device with hybrid-shaped bumpers. The NES device with wedge-shaped bumpers exhibits lower performance in dissipating and redistributing the vibration energy.

Besides the time series and wavelet spectra, standard one-sided Fourier spectra are used to strengthen the analysis of experimental results in the frequency domain. Discrete Fourier transforms are performed on the four time series shown in Fig. 14. Exponential windowing is applied to the time series to reduce the spectral leakage and suppress noise in the signal (Fladung and Rost 1997). Fig. 15 presents the Fourier spectra from 0 to 8 Hz, covering the first three modes of the structure. As shown in the figure, the first- and second-mode components are alleviated to different degrees in every case with the activated NES device. Additionally, for the NES device equipped with pyramid-shaped bumpers, the third-mode response is shown to be higher than that of the locked case. These phenomena are consistent with those observed in the wavelet spectra.

Fig. 16 presents the corresponding displacement response of the top floor with respect to the shake table, considering the same four cases shown in Figs. 14 and 15. The velocity and displacement responses are estimated based on the collected acceleration signals (Boore and Bommer 2005). The acceleration signals are filtered to remove noise and prevent unrealistic drift in the estimate. Subsequently,

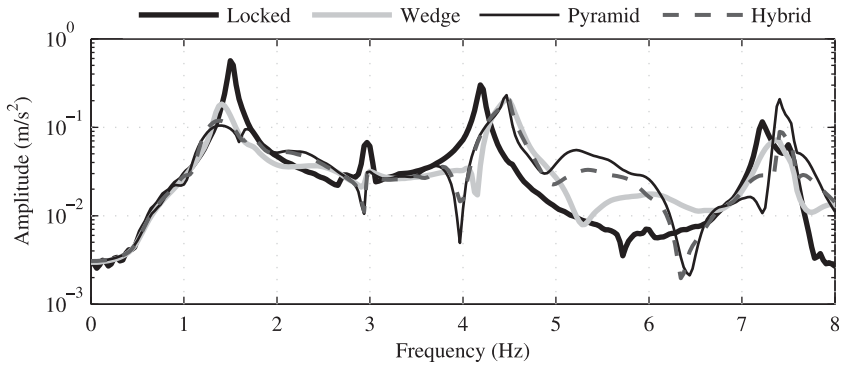

Fig. 15. Single-sided Fourier spectra of building-top acceleration from experiments with NES devices with different bumper configurations

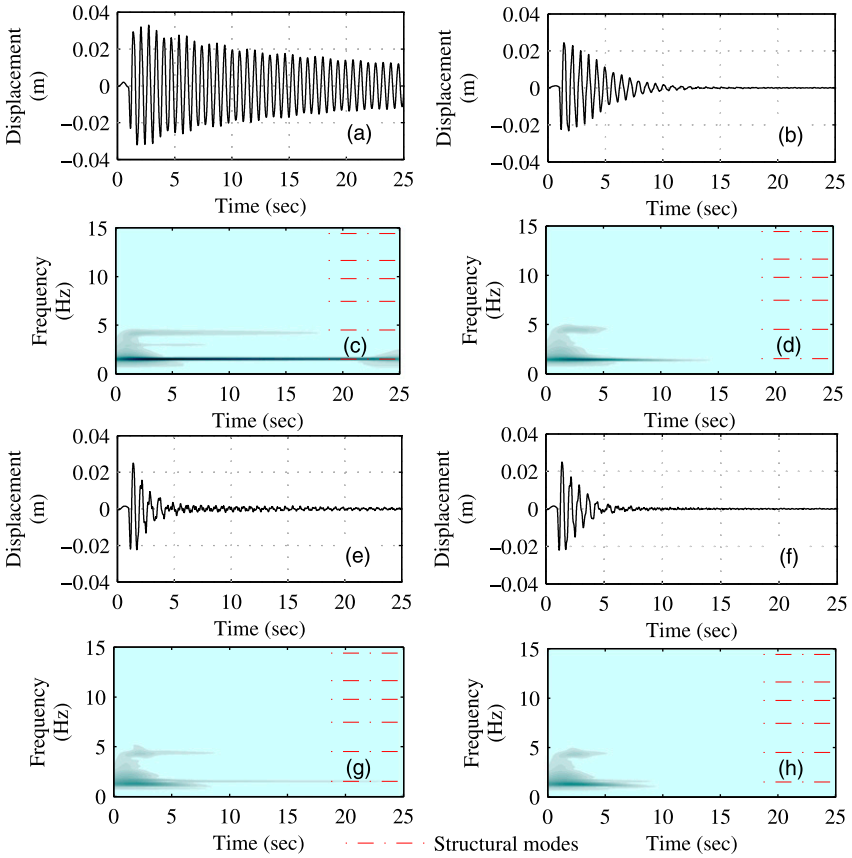

Fig. 16. Time series and wavelet spectra of building-top relative displacement from experiments with NES devices with different bumper configurations: (a) and (c) NES device locked; (b) and (d) NES device with wedge-shaped bumpers; (e) and (g) NES device with pyramid-shaped bumpers; (f) and (h) NES device with hybrid-shaped bumpers

the difference between the filtered acceleration of the top floor and the base is used as the relative acceleration and numerically integrated as the estimation of relative velocity response. The relative velocity is filtered and integrated again to obtain the relative displacement response shown in Fig. 16. The digital filters used in this procedure are described in the preceding section. As noted earlier, all three unlocked NES device configurations provide appreciable damping, and the response reduction is most pronounced for the NES device designs with pyramid- and hybrid-shaped bumpers. The time series in conjunction with wavelet spectra demonstrate that the decrease in the displacement response in the time domain mainly depends on the decay of the harmonic component of the first and second modes. This is expected because the vibration of the low-frequency modes typically contributes the major part of the total displacement response. Because of the highly alleviated first- and second-mode responses shown in Figs. 16(g and h), the time-domain displacements presented in Figs. 16(e and f) are reduced to almost zero within 5 s. However, the NES device with wedge-shaped bumpers is less capable of mitigating vibration in the first and second modes, and thus the displacement response decays much more slowly in the time domain. The robustness of the NES device performance is demonstrated by the significant response reduction that is achieved even with a NES device design that contains a lower degree of nonlinearity (wedge-shaped bumpers).

For both the acceleration and displacement responses shown in Figs. 14 and 16, although the NES device can significantly enhance the apparent structural damping, the peak responses at the very beginning are not significantly reduced. This illustrates one limitation of the type of NES device considered in this work, although alternative NES device designs incorporating nonsmooth nonlinearity currently under investigation address this issue to some degree (AL-Shudeifat et al. 2013). In the current NES device configuration, motion of the NES device mass is required for response reduction, and under impulse-like loading, the structural response reaches its peak in a very short time, which is smaller than the characteristic time scale of the NES device response. Despite this limitation, as demonstrated in this study, the NES device is capable of drastically reducing the amplitudes of the subsequent cycles and shortening the overall transient response time of the primary structure. For civil structures, various global and local failure modes under dynamic loading may be caused by cumulative damage from multiple cycles of large-amplitude vibration. Therefore, when applied to civil structures, the enhanced structural damping induced by the NES device can significantly reduce the cumulative structural response and thus may improve the chance of survival under extreme loading conditions.

The use of elastomeric bumpers is a feasible approach for realizing nonlinear restoring forces in NES device designs, and a high degree of adaptability can be obtained through the combination of material selection and geometric design. The research described in this paper is part of a comprehensive program studying NES device implementation for vibration mitigation, and additional studies related to optimization of NES device parameters for maximum response reduction are discussed elsewhere (Wierschem et al. 2012a).

Summary and Conclusions

The NES devices are innovative lightweight passive vibration absorbers that are capable of rapidly dissipating energy for vibration control and shock mitigation in mechanical and structural systems. Because of essential nonlinearity, the NES device attachment has no fixed natural frequency. Therefore, the NES device can engage with multiple modes of the primary structure to extract energy through broadband targeted energy transfer. Hence though local in nature, a NES device is capable of affecting the global dynamics of the structure to which it is attached. On the contrary, traditional linear absorber designs are only able to effectively interact with modes in a limited band of frequencies.

Although transverse linear springs have been used to realize smooth essential nonlinearity in NES devices, this approach is not necessarily realistic for implementation in large-scale structures. Hence alternative approaches for achieving essential nonlinearity are critical for transferring the NES technology into civil infrastructure systems. This research explored an innovative two-stage NES device using pairs of elastomeric polyurethane foam bumpers.

Fundamental material characterization of the elastomeric foam was conducted using quasi-static and dynamic tests. The foam was shown to exhibit stable cyclic dynamic response that was consistent with the monotonic quasi-static response. A number of foam bumpers were studied to identify the effects of geometric variations on the load-deformation behavior. Increasing the overall bumper height was shown to decrease the global bumper stiffness, and decreasing the bumper top width was shown to increase the degree of nonlinearity in the stiffness.

Nonlinear system identification of three NES device configurations (with wedge-, pyramid-, and hybrid-shaped bumpers) demonstrates that a nonlinear stiffness exponent of 3 can be achieved with hybrid-shaped bumpers, and a nonlinear stiffness exponent greater than 4 can be achieved with pyramid-shaped bumpers.

Shake-table testing using impulsive loading of a model 6-story building illustrates that NES devices with elastomeric bumpers can provide effective vibration mitigation by rapidly dissipating and redistributing high levels of input energy, although the device has only 5% of the structural mass. All three NES device configurations rapidly suppressed building acceleration. The NES device configurations with pyramid- and hybrid-shaped bumpers rapidly suppressed building displacement. In summary, elastomeric bumpers were shown to be a feasible approach for realizing nonlinear restoring forces in NES device designs and providing effective vibration mitigation in large-scale building environments.

Acknowledgments

This research program was sponsored by the Defense Advanced Research Projects Agency (DARPA) through Grant HR0011-10-1-0077 under program manager Dr. Aaron Lazarus. The content of this paper does not necessarily reflect the position or policy of the U.S. government, and no official endorsement should be inferred.

References

AL-Shudeifat, M. A., Wierschem, N., Quinn, D. D., Vakakis, A. F., Bergman, L. A., and Spencer B. F. Jr. (2013). "Numerical and experimental investigation of a highly effective single-sided vibro-impact nonlinear energy sink for shock mitigation." *Int. J. Non-Linear Mech.*, 52, 96–109.

Boore, D. M., and Bommer, J. J. (2005). "Processing of strong-motion accelerograms: Needs, options and consequences." *Soil. Dyn. Earthquake Eng.*, 25(2), 93–115.

Corsaro, R. D., and Sperling, L. H. (1990). *Sound and vibration damping with polymers*, American Chemical Society, Washington, DC.

Fladung, W., and Rost, R. (1997). "Application and correction of the exponential window for frequency response functions." *Mech. Syst. Signal Process.*, 11(1), 23–36.

Gendelman, O., Manevitch, L. I., Vakakis, A. F., and M'Closkey, R. (2000). "Energy pumping in nonlinear mechanical oscillators. I: Dynamics of the underlying Hamiltonian systems." *J. Appl. Mech.*, 68(1), 34–41.

Gent, A. N. (2001). *Engineering with rubber: How to design rubber components*, 2nd Ed., Hanser, Cincinnati.

Gibson, L. J., and Ashby, M. F. (1997). *Cellular solids: Structures and properties*, Cambridge University Press, Cambridge, U.K.

Gong, L., and Kyriakides, S. (2005). "Compressive response of open-cell foams. II: Initiation and evolution of crushing." *Int. J. Solids Struct.*, 42(5–6), 1381–1399.

Gong, L., Kyriakides, S., and Jang, W. Y. (2005). "Compressive response of open-cell foams. I: Morphology and elastic properties." *Int. J. Solids Struct.*, 42(5–6), 1355–1379.

Gourdon, E., Alexander, N. A., Taylor, C. A., Lamarque, C. H., and Pernot, S. (2007). "Nonlinear energy pumping under transient forcing with strongly nonlinear coupling: Theoretical and experimental results." *J. Sound Vibrat.*, 300(3–5), 522–551.

Kerschen, G., Kowtko, J. J., McFarland, D. M., Bergman, L. A., and Vakakis, A. F. (2007). "Theoretical and experimental study of multimodal targeted energy transfer in a system of coupled oscillators." *Nonlinear Dyn.*, 47(1–3), 285–309.

Masri, S. F., and Caughey, T. K. (1979). "A nonparametric identification technique for nonlinear dynamic problems." *J. Appl. Mech.*, 46(2), 433–447.

McFarland, D. M., Bergman, L. A., and Vakakis, A. F. (2005a). "Experimental study of non-linear energy pumping occurring at a single fast frequency." *Int. J. Non-Linear Mech.*, 40(6), 891–899.

McFarland, D. M., Kerschen, G., Kowtko, J. J., Lee, Y. S., Bergman, L. A., and Vakakis, A. F. (2005b). "Experimental investigation of targeted

energy transfers in strongly and nonlinearly coupled oscillators." *J. Acoust. Soc. Am.*, 118(2), 791–799.
Quinn, D. D., et al. (2012). "Equivalent modal damping, stiffening and energy exchanges in multi-degree-of-freedom systems with strongly nonlinear attachments." *Proc. Inst. Mech. Eng.*, 226(K2), 122–146.
Quinn, D. D., Gendelman, O., Kerschen, G., Sapsis, T. P., Bergman, L. A., and Vakakis, A. F. (2008). "Efficiency of targeted energy transfers in coupled nonlinear oscillators associated with 1:1 resonance capture: Part I." *J. Sound Vibrat.*, 311(3–5), 1228–1248.
Sapsis, T. P., Vakakis, A. F., Gendelman, O. V., Bergman, L. A., Kerschen, G., and Quinn, D. D. (2009). "Efficiency of targeted energy transfers in coupled nonlinear oscillators associated with 1:1 resonance captures. II: Analytical study." *J. Sound Vibrat.*, 325(1–2), 297–320.
Vakakis, A. F., and Gendelman, O. (2000). "Energy pumping in nonlinear mechanical oscillators. II: Resonance capture." *J. Appl. Mech.*, 68(1), 42–48.
Vakakis, A. F., Gendelman, O., Bergman, L. A., McFarland, D. M., Kerschen, G., and Lee, Y. S. (2008). *Passive nonlinear targeted energy transfer in mechanical and structural systems*, Vols. I and II, Springer, Berlin.
Vakakis, A. F., McFarland, D. M., Bergman, L. A., Manevitch, L. I., and Gendelman, O. (2004). "Isolated resonance captures and resonance capture cascades leading to single- or multi-mode passive energy pumping in damped coupled oscillators." *J. Vib. Acoust.*, 126(2), 235–244.
Wierschem, N. E., et al. (2012a). "Experimental testing and simulation of a 6-story structure incorporating a coupled two mass nonlinear energy sink." *J. Struct. Eng.*, in press.
Wierschem, N. E., et al. (2012b). "Passive damping enhancement of a two-degree-of-freedom system through a strongly nonlinear two-degree-of-freedom attachment." *J. Sound Vibrat.*, 331(25), 5393–5407.
Wierzbicki, T., and Doyoyo, M. (2003). "Determination of local-stress response of foams." *J. Appl. Mech.*, 70(2), 204–211.